ADVANCED ELECTRONIC MATERIALS
www.advelectronicmat.de

Ferroelastic-Domain-Assisted Mechanical Switching of Ferroelectric Domains in $Pb(Zr,Ti)O_3$ Thin Films

*Guoliang Yuan, Houbing Huang, Chen Li, Di Liu, Zhihao Cheng, and Di Wu**

A recent breakthrough in mechanical polarization switching provides a valuable handle to achieve nanoscale ferroelectric domain control. This flexoelectric switching is usually observed in ultrathin films (≈10 nm or less in thickness), where a large strain gradient is possible. However, from the point of view of device applications, it will be more attractive to achieve mechanical domain switching in thicker films. Here, it is experimentally demonstrated that by introducing ferroelastic a-domains in $PbZr_{0.1}Ti_{0.9}O_3$ films the potential barrier against 180° c-domain switching can be greatly decreased, enabling mechanical ferroelectric domain switching in 50 nm thick films by applying a loading force from an atomic force microscope tip. Moreover, these a-domains are stable in the c-domain matrix without further mechanical stressing. This makes it possible to create nanoscale domain wall circuitry. These results shed light on the mechanism of domain switching in ferroelectric thin films and may facilitate the design of mechanically controlled novel ferroelectric devices.

1. Introduction

Ferroelectric thin films have been widely used in piezoelectric sensors, actuators, surface acoustic wave devices, and nonvolatile memories.[1] Functions of these devices rely on the control of polarization and hence the domain structures. Recently, domain-wall nanoelectronics have attracted much attention in many oxide ferroelectric films such as $PbZr_{1-x}Ti_xO_3$,[2–9] $BiFeO_3$,[10–13] and $AMnO_3$ (A = Y, Bi, and Er),[14] which further require precise control of domain and domain walls on the nanometer scale for domain circuitry.[15] For tetragonal $PbZr_{1-x}Ti_xO_3$ thin films, there are **c**-domains with the out-of-plane polarization in the [001] direction and **a**-domains with in-plane polarization in the [010] and [100] crystallographic directions.[3–8] Feigl et al. observed that the **a**/**c** domain walls in $PbZr_{0.1}Ti_{0.9}O_3$ (PZT) are more conductive than the domains themselves.[3] Stolichnov et al. discovered nonthermally activated metallic-like conductivity along the **a**/**c** domain walls in PZT films deposited on (001) $DyScO_3$ (DSO).[2] These observations provide the opportunity to fabricate high-density devices based on modulating the conductivity of domain walls. The width and density of these **a**-domains can be manipulated to some extent by tuning the film thickness and the epitaxial strain imposed by the substrate during the epitaxial film growth.[16] However, to precisely control domain width, orientation and position by external electric field or mechanical force are more challenging and rather new topic since this ability provides a valuable handle to prepare domain wall circuitries in the nanometer scale for future devices.[15]

Recently, Lu et al. accomplished 180° polarization switching in 4.8 nm thick tetragonal $BaTiO_3$ thin films by applying a mechanical force through a tip in contact with the film surface in an atomic force microscope.[17–22] This breakthrough provides tremendous opportunities to develop mechanical manipulation of domain structures for novel electronic devices.[15,17,23,24] For example, a mechanically controlled ferroelectric tunnel junction memory has been proposed.[17] This mechanical switching is a demonstration of flexoelectric effect, in which a strain gradient, imposed by the tip, produces an effective electric field that switches the polarization.[18,25] The flexoelectric coefficient $f \sim e/a$, where e is the electronic charge and a is the lattice constant, is quite small (in the order of nC m^{-1}).[26,27] This effect is usually negligible in thick films but prominent in films of several nanometers in thickness because of the large strain gradient (≈10^8 m^{-1}) that can be achieved. However, it is challenging to achieve high quality ferroelectric thin films with a thickness of less than 10 nm by a cost-effective method. In fact, commercial ferroelectric devices such as memories still focus on thicker films to ensure their fatigue-free characteristic and other reliabilities, and hence a high performance. Therefore, the pursuit of

Prof. G. Yuan, Dr. C. Li, Z. Cheng, Prof. D. Wu
National Laboratory of Solid State Microstructures
Department of Materials Science and Engineering
and Collaborative Innovation Center for Advanced Microstructures
Nanjing University
Nanjing 210093, China
E-mail: diwu@nju.edu.cn
Prof. G. Yuan, Z. Cheng
School of Materials Science and Engineering
Nanjing University of Science and Technology
Nanjing 210094, China
Prof. H. Huang, D. Liu
School of Materials Science and Engineering
Beijing Institute of Technology
Beijing 100081, China
Dr. C. Li, Prof. D. Wu
Jiangsu Key Laboratory of Artificial Materials
Nanjing University
Nanjing 210093, China
The ORCID identification number(s) for the author(s) of this article can be found under https://doi.org/10.1002/aelm.202000300.

DOI: 10.1002/aelm.202000300

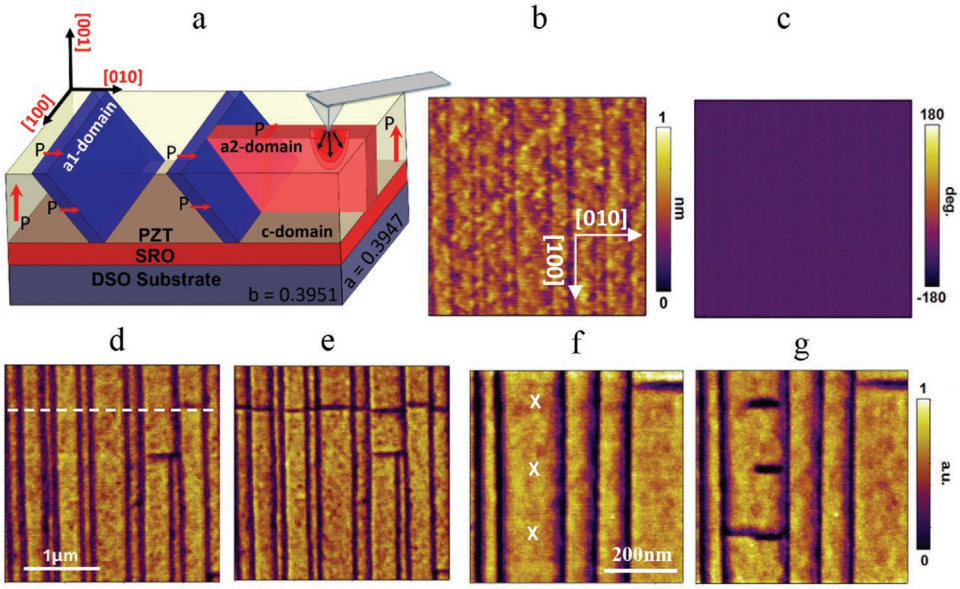

Figure 1. Domain structure of (001) PZT film on DSO substrate. a) A sketch of the a/c multidomain structure, where the red arrows indicate the polarization direction in each domain. b,c) Atomic force microscope image and out-of-plane PFM phase image of the PZT film, respectively. d,e) PFM amplitude images acquired before and after scanning the PFM tip, with 1200 nN loaded, along the white dash line in (c). f,g) PFM amplitude images acquired before and after pressing the PFM tip, with 1000 nN loaded, on the three points indicated by the white crosses one by one.

mechanical switching in thicker films may be valuable due to better performance, higher reliability and easier fabrication.

2. Results and Discussion

Here we show that the potential barrier of 180° polarization switching can be effectively decreased by introducing metastable **a**-domains in PZT films, which makes the flexoelectric switching possible in films as thick as 50 nm. Furthermore, the domain patterns and the conductive a/c domain walls can be precisely manipulated by a mechanical force or an electric field, which is required for designing of novel electronic devices.

The 50 nm thick PZT films were deposited on ScO_2- and TiO_2-terminated (001) $DyScO_3$ (DSO) and $SrTiO_3$ (STO) substrates, respectively, with a 15 nm thick $SrRuO_3$ (SRO) buffer layer by pulsed laser deposition (i.e., PZT/SRO/DSO and PZT/SRO/STO; see Figure S1 in the Supporting Information).[28,29] **Figure** 1a shows the structure of PZT/SRO/DSO, where crystallographic planes and directions of DSO were indexed according to a pseudocubic structure for easy comparison. 2D X-ray diffraction intensity recorded around the (103) reciprocal spot of the substrate suggest high-quality epitaxy on both DSO and STO substrates without lattice relaxation (see Figure S2 in the Supporting Information). PZT film thickness estimated from diffraction intensity fringes is about 50 nm on both substrates.

Figure 1b shows the surface morphology of the PZT thin film of PZT/SRO/DSO. The surface is smooth with a root-mean-square roughness about 0.14 nm over a 3×3 μm^2 square. However, straight dark stripes along [100] and [010] directions can be clearly observed, indicating shallow trenches on the surface. Figure 1c,d shows the corresponding out-of-plane piezoresponse force microscopy (PFM) phase and amplitude images. It is observed that these dark stripes show no response to the out-of-plane stimulus while the rest of the film shows a uniform PFM response in the amplitude image. However, these stripes show a clear in-plane PFM response (see Figure S3 in the Supporting Information). Thus, these PZT films are composed of **a**-domains without the out-of-plane PFM response embedded in a **c**-domain matrix, as shown schematically in Figure 1a. Following convention,[3,30] the long stripes along [100] are denoted as **a**1-domains while the short stripes along [010] **a**2-domains. At room temperature, PZT shows a tetragonal structure with $a = b = 0.3914$ nm and $c = 0.4138$ nm, while the DSO substrate is pseudocubic with in-plane lattice parameters $a = 0.3947$ nm and $b = 0.3951$ nm.[31] Therefore, PZT **c**-domains are stable in compressive strain or small tensile strain in both in-plane directions while **a**-domains become stable in a large tensile strain. Lu et al. reported that a1/a2 domain structure gradually becomes stable once the epitaxial tensile strain is larger than >0.3% for the pure $PbTiO_3$ film.[32] As pointed out previously, this **a**/**c** multidomain structure appears as a result of minimized elastic energy because the tensile strain can be relaxed at the **a**/**c** domain boundary.[3,8,30] Each dark stripe represents one **a**-domain and two **a**/**c** domain boundaries.[3] In these 50 nm thick PZT films, the **a**-domains are about ≈10 nm in width. It is also noticed that the population of long **a**1-domains along [010] is much larger than that of short **a**2-domains along [100] in the as-deposited PZT films, implying that **a**1-domains are energetically more favorable than **a**2-domains due to the anisotropy in in-plane lattice parameters in DSO. The uniform out-of-plane PFM phase contrast in Figure 1c indicates that the polarizations in all the **c**-domains are aligned in the same direction. These **c**-domains can be switched by a positive voltage applied to the film surface (see Figure S4 in the Supporting Information). Therefore, **c**-domains in the as-deposited film exhibit a polarization pointing to the film surface and are hereafter labeled as +**c**-domains. For comparison, the PZT film of PZT/SRO/STO

exhibits a single +**c**-domain state with the polarization pointing to the film surface (see Figure S4 in the Supporting Information). Since the in-plane lattice parameters of PZT is larger than those of STO, which is in cubic structure with $a = 0.3905$ nm, the 0.23% compressive epitaxial strain in PZT favors the +**c** polarization which can be switched to −**c** only by a positive voltage applied on the film surface.

We demonstrate that **a**-domains can be created in these PZT films by applying a mechanical force on the film surface. After the film was scanned by the tip with a constant load of 1200 nN along the dash line in Figure 1d, **a**2-domains appear along the trace of the tip movement over an area where only **a**1/**c** domains exist before the scan (Figure 1d,e). **a**2-domains can also be created at a prescribed position by pressing the tip with a certain force on the surface of +**c**-domains. As shown in Figure 1f,g, three **a**2-domains are created one by one by pressing the tip with 1000 nN at the points indicated by the white crosses. These **a**2-domains may extend along the [010] direction until they are stopped at **a**1-domain boundaries.[3,4] Khan et al. reported that **a**-domains appear in PZT after scanning an electrically biased tip in contact with the surface.[33] The creation of **a**-domains by a mechanical force resembles the creation by an electric field. The applied mechanical force increases the energy of the +**c**-domain through the flexoelectric coupling and **a**2-domains appear to lower the total energy.[31] Since the nanoscale **a**/**c** domain walls of the PZT film show metallic-like conductivity according to previous studies,[2,3] their precise control is an important step to design and prepare domain wall circuitries in future.[15]

We then show that the +**c**-domains in the 50 nm thick PZT films can be switched by 180° through application of a mechanical force. **Figure 2** displays out-of-plane PFM phase and amplitude images acquired after scanning with the tip under different loading forces. The fast scan direction is along [010] (from left to right in Figure 2) and the slow scan direction is along [100] (from top to bottom in Figure 2). After scanning by the conductive tip with a constant force of 1375 nN, there are only a few tiny −**c** nuclei (≈40 nm in size) observed in the phase image. In the corresponding amplitude image, a large number of **a**2-domains and a few **a**1-domains appear in the +**c**-domain matrix.[34] As the force increases to 1880 nN, 180° domain switching occurs and −**c**-domains appear at the top of the scanned area (Figure 2e,f). With the force further increased, −**c**-domains grow by pushing the −**c**/+**c** domain wall along the slow scan direction consuming the area occupied by the +**c**-domains (Figure 2g,h). It is observed that **a**2-domains left in −**c**-domain matrix are erased by the subsequent scans. At 2730 nN, the uniform PFM phase contrast opposite to that in the as-deposited film (Figure 2a) indicates the completion of the mechanical switching in the scanned area. In this switching process, the erasure of **a**2-domains implies that these domains are metastable. The +**c** → −**c** switching process is dominated by −**c**/+**c** domain wall motion along [100], while nucleation of −**c**-domains is rarely observed. Subsurface defects may act as pinning sites for moving domain walls.[35] The creep motion of domain walls under an external field is a competition between the tendency to lower the elastic energy of a moving domain wall and the retardation from the defect pinning potential.[36] It has been observed that strain fields in thin films has a great effect on the velocity of domain motion.[37] The appearance of the metastable ferroelastic domains before ferroelectric domain switching relaxes the strain and lowers the local elastic energy in PZT.[30,33] This may help to promote the propagation of −**c**/+**c** domain wall.

The mechanical switching of **c**-domains is anisotropic in a sense that it depends on the fast scan direction. As shown in **Figure** 3a–d, when the fast scan direction of the mechanical load is set along [100], together with **a**-domains created, a large number of −**c** nuclei appear all around in the area scanned with 1100 nN. This is in agreement with previous reports that the appearance of **a**-domains may help the nucleation of −**c**-domains in the tetragonal ferroelectric film such as

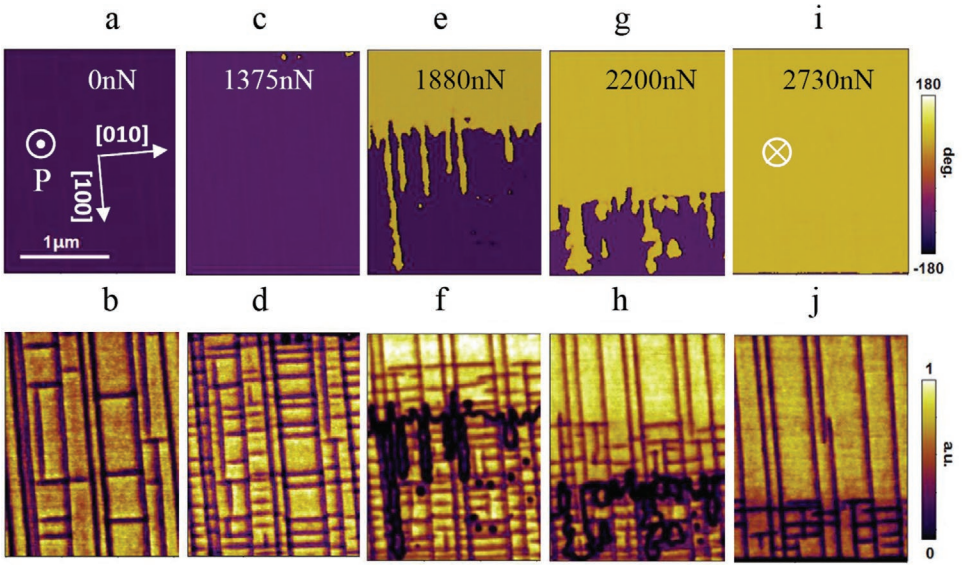

Figure 2. Domain evolution under an increasing force (fast scan along [010]). PFM phase and amplitude images of the as-grown film a,b), and the same film after it was scanned with the constant loading forces of 1375 nN c,d), 1880 nN e,f), 2200 nN g,h), and 2730 nN i,j) applied to the tip.

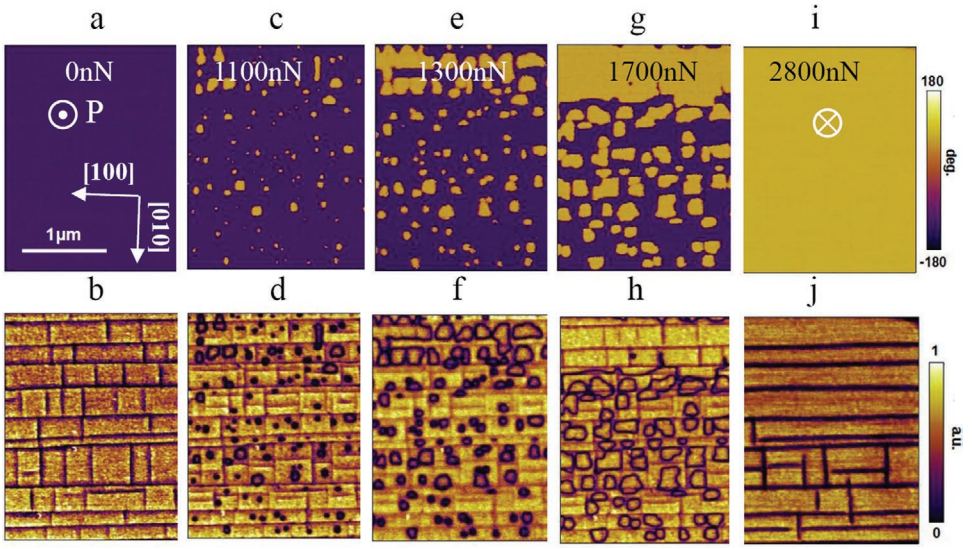

Figure 3. Domain evolution with increasing force (fast scan along [100]). PFM phase and amplitude images before the mechanical scan a,b), and after scanning with 1100 nN c,d), 1300 nN e,f), 1700 nN g,h), and 2800 nN i,j) loaded on the tip.

$BaTiO_3$ and PZT.[5] Experiments and phase-field simulations have revealed that opposite domains in PZT films nucleate preferentially along **a**-domains in a **c**-domain matrix, due to the localized reduction of electrostatic and elastic contributions to the nucleation potential.[5,34,38] With increasing the loading force step by step to 2800 nN, these **−c** nuclei grow and coalesce to complete the switching (Figure 3e–j). This is in contrast to the switching pattern observed with the fast scan direction along [010] in Figure 2, where the switching is predominantly controlled by the domain wall motion. Gao et al. reported that **a**-domains in PZT might hinder the propagation of the **−c**/**+c** domain walls.[5] As shown in Figure 3e,f, **−c**-domains are indeed confined within small rectangles enclosed by **a**1- and **a**2-domains after scanned with 1300 nN. However, these obstacles could be overcome by applying a stronger force (Figure 3g–j). Compared with images shown in Figure 2, one may observe that **a**1-domains exhibit a higher energy barrier against the motion of **−c**/**+c** domain wall than **a**2-domains. Therefore, **−c**/**+c** domain wall motion along the **a**1-domains is easier than that across the **a**1-domains.

Khan et al. have previously reported the creation and elimination of **a**-domains in PZT by scanning with an electrically biased tip.[33] In the present study, one may observe, from the mechanical switching above, that these **a**-domains appear to help the ferroelectric **c**-domain switching. We show that the **c**-domain switching process by applying a mechanical force is the same as applying an electrical field. As shown in **Figure 4**, after the PZT/SRO/DSO film is scanned with a tip biased at 2.3 V, a number of **a**2-domains were created. Under the positive bias at the tip, the electrostatic energy of **+c**-domains increases and **a**/**c** multidomain structure appears to lower the energy. Although these created ferroelastic **a**2-domains are metastable, they may remain intact for 24 h after the bias is released (see Figure S5 in the Supporting Information). With the increase of the electric bias, **−c**-domains nucleate and grow by pushing forth the **−c**/**+c** domain wall along the [100] direction, i.e., along the slow scan direction (Figure 4e,f). Almost all **+c**-domains are consumed after the scan with the tip under 4.0 V, although some **a**2-domains are left inside the **−c**-domains (Figure 4g,h). These metastable **a**2-domains are eliminated by a subsequent scan with 6.0 V tip bias (Figure 4i,j).

The polarization switching in PZT/SRO/STO and PZT/SRO/DSO is compared to better understand the effect of epitaxial strain on the switching process. The as-grown PZT film on the STO substrate is in a single **+c**-domain state (see Figure S4 in the Supporting Information). Although **−c** nuclei have not been observed after the scanning with a tip with 2735 nN load, this single **+c**-domain PZT can be switched by scanning with an electrically biased tip. It is observed that **−c**-domain nuclei appear at 8.0 V tip bias and the switching is completed after scanning with a 12.0 V tip bias (see Figure S6 in the Supporting Information). Figure 4k,l shows the PFM phase and amplitude hysteresis versus tip bias loops of the PZT film on the STO substrate, respectively. The coercive voltage is about ±(12.0–14.0) V, as indicated by the two minima in the amplitude loops. Phase-field simulation is applied to understand the one-step **+c** → **−c** polarization switching in PZT/SRO/STO. Because there is 0.23% compressive strain in PZT film deposited on the (001) STO substrate, only **c**-domains are stable (see Figure S7 in the Supporting Information), while **a**-domains are not allowed to appear due to the large elastic energy penalty. As a result, just direct one-step **+c** → **−c** switching is possible and the coercive field is large according to the normalized polarization/strain versus electric field loops in **Figure** 5a,b.

On the contrary, the **a**/**c** multidomain structure greatly lowers the potential barrier against 180° **+c** → **−c** polarization switching in DSO/SRO/PZT.[19,39,40] The coercive voltage of PZT/SRO/DSO is much smaller, about only ±(3.0–4.0) V (Figure 4k,l). Furthermore, the normalized polarization and strain versus electric field curves are achieved from our phase-field simulation.[41,42] The corresponding coercive field of the

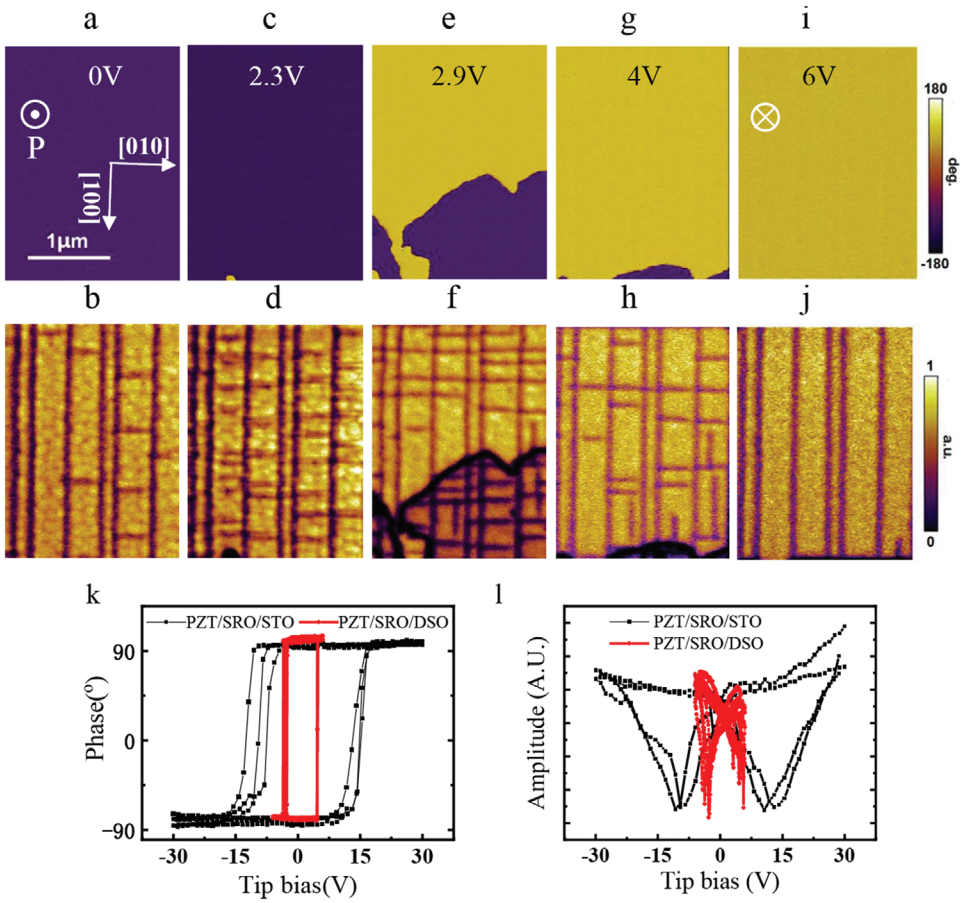

Figure 4. Polarization switching and domain evolution under external voltage. PFM phase and amplitude images of the PZT/SRO/DSO before a,b), and after the tip scanning (fast scan along [010]) with 2.3 V c,d), 2.9 V e,f), 4.0 V g,h), and 6.0 V i,j) bias. k) Phase and l) amplitude versus tip bias curves of PZT/SRO/STO and PZR/SRO/DSO.

PZT film on DSO is only 30% of that on STO (Figure 5a,b), which is consistent with the coercive voltages measured by PFM discussed above. Figure 5 shows phase-field simulation results illustrating evolution of the domain structures during polarization switching with respect to the polarization hysteresis. The domain evolution shows the +**c** → **a**1/**a**2 → −**c** two-step polarization switching in detail (Figure 5c,d). Deposited on (001) DSO substrates, PZT films are imposed of 0.84% tensile strain along [100] direction and 0.95% tensile strain along [010] direction. Therefore, **a**-domains should be energetically favorable than **c**-domains (see Figure S8 in the Supporting Information). However, in our 50 nm thick PZT, the epitaxial tensile strain may relax. If the tensile strain is relaxed to ≈0.5%, the minimum Gibbs free energy of ±**a**1-, ±**a**2- and ±**c**2-domains are close to each other and all of them can coexist.[32] The energy barrier of the two-step +**c** → **a**1/**a**2 → −**c** polarization switching is much lower than that of the one-step +**c** → −**c** switching, thus the appearance of metastable **a**-domains lowers the effective barrier.[34] Both PFM experiments and phase-field simulation prove that the +**c** → −**c** polarization switching is much easier in the **a**/**c** multidomain PZT than in the +**c** single domain PZT, thus **a**1/**a**2 domains indeed help the nucleation of **c** anti-domain.[34] As a result, the two-step +**c** → **a**1/**a**2 → −**c** polarization switching can be completed with a much smaller driving force, facilitating a pure mechanical force switching in thicker films.

3. Conclusion

In summary, mechanical **c**-domain switching has been achieved in **a**/**c** multidomain PZT films as thick as 50 nm by scanning with the tip under an applied load. The mechanical switching process is essentially the same as an electric switching by scanning with a biased tip, indicating that the strain gradient imposed by the tip produces an effective electric field through the flexoelectric effect and then drives the ferroelectric domain switching. A number of **a**-domains nucleate and grow in the +**c**-domain matrix. This greatly lowers the switching barrier and facilitates a two-step polarization switching of +**c** → −**c** through formation of a metastable intermediate multidomain state, making the mechanical switching possible in relatively thick films. More interestingly, since **a**-domains can be created at a prescribed position by simply applying either a mechanical force or an electric field through the tip and there are the relatively high conductivity in **a**/**c** domain walls, this nanoscale domain manipulation may find applications in making complex nanometer-scale circuitries for future domain wall electronic.

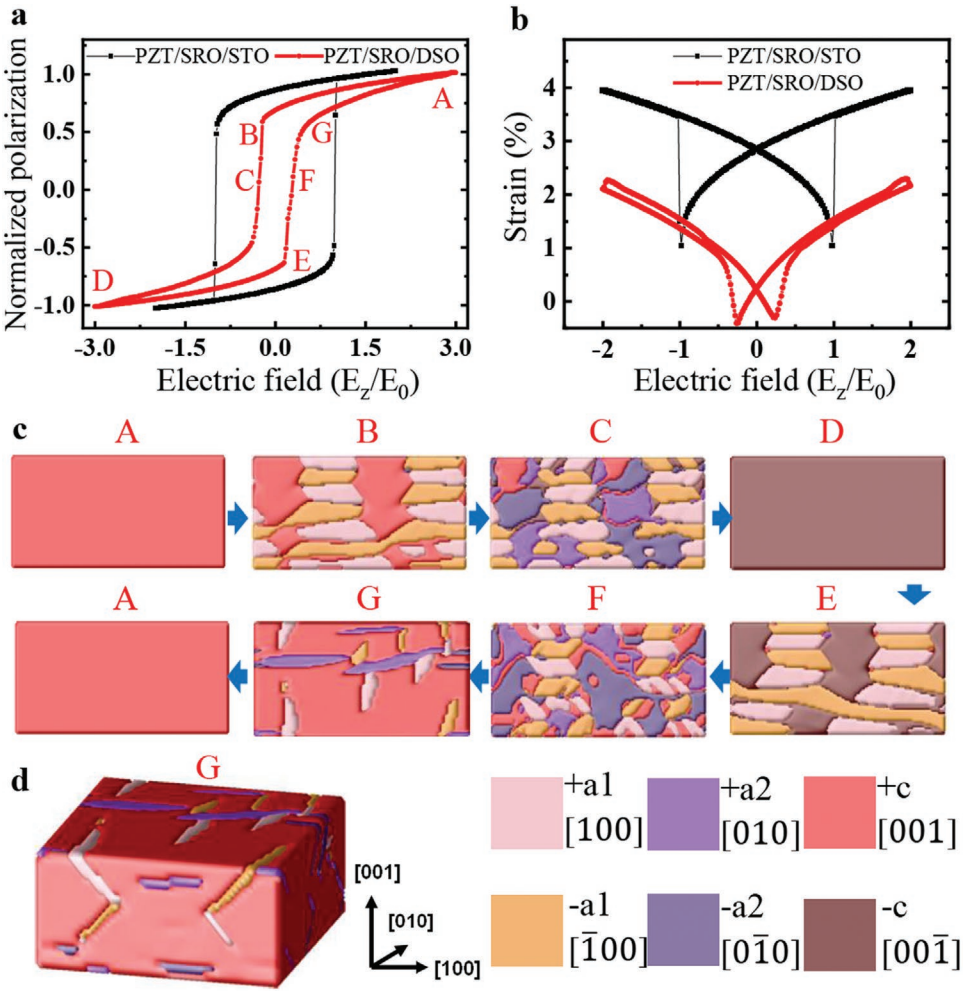

Figure 5. Polarization switching and domain evolution from phase-field simulations. a) Normalized polarization and b) strain versus electric field loops and c) 2D and d) 3D domain patterns in PZT/SRO/DSO, where *Ez* is the electric field along (001) and E_0 is 1.25×10^8 V m^{-1}, and the A-G in (c) and (d) correspond to seven points in the switching hysteresis shown in (a).

4. Experimental Section

Sample Preparation: (001) STO and DSO substrates were etched in NH_4F-buffered HF solution and annealed at 950 and 1000 °C, respectively, in flowing oxygen to achieve TiO_2- and ScO_2-terminated surface. SRO electrodes and PZT films were deposited in sequence on the (pseudo) cubic (001) surface of the substrate by pulsed laser deposition (Adanano Tech.) using a KrF (λ = 248 nm) excimer laser (Coherent COMPexPro 205). The laser energy density used was about 1.0 J cm^{-2} and the O_2 pressure was kept at 0.1 mbar. Deposition temperature was 625 °C for SRO and 575 °C for PZT.

Crystal Structure and Properties Characterization: The crystal structures of PZT heterostructures were characterized using high-resolution X-ray diffraction at BL14B1-XRD beam line (λ = 0.12398 nm) of Shanghai Synchrotron Radiation Facility (China). The surface morphology and ferroelectric properties were measured using an Asylum Research Cypher scanning probe microscope. Conductive Cr/Pt/Ir-coated tips (Nanoworld EFM), with a nominal force constant about 2.8 N m^{-1} and a 30 nm tip radius, were used for the mechanical switching, the electric switching, and the PFM measurement. Hysteresis loops were measured in the dual a.c. resonance tracking (DART) mode with pulses following a triangle profile applied on the tip. The phase and amplitude data were acquired with a 0.5 V a.c. bias. Single-frequency PFM mode was used for phase and amplitude images. The tip load is 30 nN for conventional electric switching and PFM measurements.

Phase-Field Simulations: During the phase-field simulations of polarization switching under an electric field or a mechanical load applied by the AFM conductive tip, polarization vector P_i = (P_1, P_2, and P_3) was used as the order parameter to describe the ferroelectric state in the PZT thin film. The temporal evolution of P_i was calculated by minimizing the total Gibbs free energy *F* via numerically solving the time-dependent Landau–Ginzburg–Devonshire (LGD) equation

$$\frac{\partial P_i(x,t)}{\partial t} = -L\frac{\partial F}{\partial P_i(x,t)}(i = 1, 2, 3) \quad (1)$$

where *x* is the spatial position (with *x*-, *y*-, *z*-axes along the [100], [010], and [001] Cartesian coordinate directions), *t* is the time, and *L* is the kinetic coefficient related to the domain wall mobility. The total free energy *F* of the PZT thin film includes the Landau, gradient, elastic, electrostatic, and flexoelectric energies. Equation (1) is numerically solved using a semi-implicit spectral method based on a 3D geometry sample with $128\Delta x \times 128\Delta y \times 32\Delta z$ size, with $\Delta x = \Delta y = \Delta z = 1.0$ nm. The thickness of the film, substrate, and air is $20\Delta z$, $10\Delta z$, and $2\Delta z$, respectively. The temperature is *T* = 25 °C, and an isotropic relative

dielectric constant is chosen to be 50. The gradient-energy coefficients are set to be $G_{11}/G_{110} = 0.6$, while $G_{110} = 1.73 \times 10^{-10}$ m^4 N C^{-2}. The Landau coefficients, electrostrictive coefficients, and elastic-compliance constants are collected from the previous study.

Supporting Information

Supporting Information is available from the Wiley Online Library or from the author.

Acknowledgements

G.Y. and H.H. contributed equally to this work. The work was supported by the Natural Science Foundation of China (51725203, 51721001, U1932115, 51790492, 51972028, 51702153 and 61874055) and by the Natural Science Foundation of Jiangsu Province (BK20160627).

Conflict of Interest

The authors declare no conflict of interest.

Keywords

ferroelastic domains, flexoelectrics, mechanical domain switching

Received: March 21, 2020
Published online:

[1] J. F. Scott, *Science* **2007**, *315*, 954.
[2] I. Stolichnov, L. Feigl, L. J. McGilly, T. Sluka, X. K. Wei, E. Colla, A. Crassous, K. Shapovalov, P. Yudin, A. K. Tagantsev, N. Setter, *Nano Lett.* **2015**, *15*, 8049.
[3] L. Feigl, P. Yudin, I. Stolichnov, T. Sluka, K. Shapovalov, M. Mtebwa, C. S. Sandu, X. K. Wei, A. K. Tagantsev, N. Setter, *Nat. Commun.* **2014**, *5*, 4677.
[4] L. Feigl, L. J. McGilly, C. S. Sandu, N. Setter, *Appl. Phys. Lett.* **2014**, *104*, 172904.
[5] P. Gao, J. Britson, J. R. Jokisaari, C. T. Nelson, S. H. Baek, Y. R. Wang, C. B. Eom, L. Q. Chen, X. Q. Pan, *Nat. Commun.* **2013**, *4*, 2791.
[6] W. Li, M. Alexe, *Appl. Phys. Lett.* **2007**, *91*, 262903.
[7] V. Nagarajan, A. Roytburd, A. Stanishevsky, S. Prasertchoung, T. Zhao, L. Chen, J. Melngailis, O. Auciello, R, R , *Nat. Mater.* **2003**, *2*, 43.
[8] A. H. G. Vlooswijk, G. Catalan, A. Janssens, B. Barcones, S. Venkatesan, G. Rijnders, B. Kooi, J. T. M de Hosson, D. H. A. Blank, B. Noheda, *Appl. Phys. Lett.* **2007**, *91*, 112901.
[9] J. Guyonnet, I. Gaponenko, S. Gariglio, P. Paruch, *Adv. Mater.* **2011**, *23*, 5377.
[10] Y. H. Chu, C. H. Yang, P. L. Yang, J. X. Zhang, K. Lee, P. Yu, L. Q. Chen, R. Ramesh, *Adv. Mater.* **2007**, *19*, 2662.
[11] Y. H Chu, Q. He, C. H. Yang, P. Yu, L. W. Martin, P. Shafer, R. Ramesh, *Nano Lett.* **2009**, *9*, 1726.
[12] J. Seidel, L. W. Martin, Q. He, Q. Zhan, Y. H. Chu, A. Rother, M. E. Hawkridge, P. Maksymovych, P. Yu, M. Gajek, N. Balke, S. V. Kalinin, S. Gemming, F. Wang, G. Catalan, J. F. Scott, N. A. Spaldin, J. Orenstein, R. Ramesh, *Nat. Mater.* **2009**, *8*, 229.
[13] S. Y. Yang, J. Seidel, S. J. Byrnes, P. Shafer, C. H. Yang, M. D. Rossell, P. Yu, Y. H. Chu, J. F. Scott, J. W. Ager, L. W. Martin, R. Ramesh, *Nat. Nanotechnol.* **2010**, *5*, 143.
[14] D. Meier, J. Seidel, A. Cano, K. Delaney, Y. Kumagai, M. Mostovoy, N. A. Spaldin, R. Ramesh, M. Fiebig, *Nat. Mater.* **2012**, *11*, 284.
[15] G. Catalan, J. Seidel, R. Ramesh, J. F. Scott, *Rev. Mod. Phys.* **2012**, *84*, 119.
[16] O. Nesterov, S. Matzen, C. Magen, A. H. G. Vlooswijk, G. Catalan, B. Noheda, *Appl. Phys. Lett.* **2013**, *103*, 142901.
[17] H. Lu, D. J. Kim, C. W. Bark, S. Ryu, C. B. Eom, E. Y. Tsymbal, A. Gruverman, *Nano Lett.* **2012**, *12*, 6289.
[18] H. Lu, C. W. Bark, D. E. De Los Ojos, J. Alcala, C. B. Eom, G. Catalan, A. Gruverman, *Science* **2012**, *336*, 59.
[19] E. J. Guo, R. Roth, S. Das, K. Dorr, *Appl. Phys. Lett.* **2014**, *105*, 012903.
[20] Y. Heo, B. K. Jang, S. J. Kim, J. Seidel, *Adv. Mater.* **2014**, *26*, 7568.
[21] Y. J. Li, J. J. Wang, J. C. Ye, X. X. Ke, G. Y. Gou, Y. Wei, F. Xue, J. Wang, C. S. Wang, R. C. Peng, X. L. Deng, Y. Yang, X. B. Ren, L. Q. Chen, C. W. Nan, J. X. Zhang, *Adv. Funct. Mater.* **2015**, *25*, 3405.
[22] Z. F. Wen, X. B. Qiu, C. Li, C. Y. Zheng, X. H. Ge, A. D. Li, D. Wu, *Appl. Phys. Lett.* **2014**, *104*, 042907.
[23] W. Z. Wu, L. Wang, Y. L. Li, F. Zhang, L. Lin, S. M. Niu, D. Chenet, X. Zhang, Y. F. Hao, T. F. Heinz, J. Hone, Z. L. Wang, *Nature* **2014**, *514*, 470.
[24] S. H. Baek, H. W. Jang, C. M. Folkman, Y. L. Li, B. Winchester, J. X. Zhang, Q. He, Y. H. Chu, C. T. Nelson, M. S. Rzchowski, X. Q. Pan, R. Ramesh, L. Q. Chen, C. B. Eom, *Nat. Mater.* **2010**, *9*, 309.
[25] B. C. Jeon, D. Lee, M. H. Lee, S. M. Yang, S. C. Chae, T. K. Song, S. D. Bu, J. S. Chung, J. G. Yoon, T. W. Noh, *Adv. Mater.* **2013**, *25*, 5643.
[26] P. Zubko, G. Catalan, *Phys. Rev. Lett.* **2007**, *99*, 167601.
[27] P. Zubko, G. Catalan, A. K. Tagantsev, *Annu. Rev. Mater. Res.* **2013**, *43*, 387.
[28] M. Kawasaki, K. Takahashi, T. Maeda, R. Tsuchiya, M. Shinohara, O. Ishiyama, T. Yonezawa, M. Yoshimoto, H. Koinuma, *Science* **1994**, *266*, 1540.
[29] J. E. Kleibeuker, G. Koster, W. Siemons, D. Dubbink, B. Kuiper, J. L. Blok, C. H. Yang, J. Ravichandran, R. Ramesh, A. T. Elshof, D. Blank, G. Rijnders, *Adv. Funct. Mater.* **2010**, *20*, 3490.
[30] W. Pompe, X. Y. Gong, Z. G. Suo, J. Speck, *J. Appl. Phys.* **1993**, *74*, 6012.
[31] B. Velickov, V. Kahlenberg, R. Bertram, M. Bernhagen, *Z. Kristallogr.* **2007**, *222*, 466.
[32] X. Y. Lu, Z. H. Chen, Y. Cao, Y. L. Tang, R. J. Xu, S. Saremi, Z. Zhang, L. You, Y. Q. Dong, S. Das, H. B. Zhang, L. M. Zheng, H. P. Wu, W. M. Lv, G. Q. Xie, X. J. Liu, J. Y. Li, L. Chen, L. Q. Chen, W. W. Cao, L. W. Martin, *Nat. Commun.* **2019**, *10*, 3951.
[33] A. I. Khan, X. Marti, C. Serrao, R. Ramesh, S. Salahuddin, *Nano Lett.* **2015**, *15*, 2229.
[34] R. J. Xu, S. Liu, I. Grinberg, J. Karthik, A. R. Damodaran, A. M. Rappe, L. W. Martin, *Nat. Mater.* **2015**, *14*, 79.
[35] T. J. Yang, U. Mohideen, V. Gopalan, P. Swart, *Phys. Rev. Lett.* **1999**, *82*, 4106.
[36] T. Tybell, P. Paruch, T. Giamarchi, J. M. Triscone, *Phys. Rev. Lett.* **2002**, *89*, 097601.
[37] E. J. Guo, R. Roth, A. Herklotz, D. Hesse, K. Dörr, *Adv. Mater.* **2015**, *27*, 1615.
[38] S. Jesse, B. J. Rodriguez, S. Choudhury, A. P. Baddorf, I. Vrejoiu, D. Hesse, M. Alexe, E. A. Eliseev, A. N. Morozovska, J. X. Zhang, L. Q. Chen, S. V. Kalinin, *Nat. Mater.* **2008**, *7*, 209.
[39] S. H. Baek, C. M. Folkman, J. W. Park, S. Lee, C. W. Bark, T. Tybell, C. B. Eom, *Adv. Mater.* **2011**, *23*, 1621.
[40] L. F. Chen, Z. H. Cheng, W. T. Xu, X. J. Meng, G. L. Yuan, J. M. Liu, Z. G. Liu, *Sci. Rep.* **2016**, *6*, 19092.
[41] L. Q. Chen, J. Shen, *Comput. Phys. Commun.* **1998**, *108*, 147.
[42] M. Haun, E. Furman, S. J. Jang, H. A. McKinstry, L. E. Cross, *J. Appl. Phys.* **1987**, *62*, 3331.

